Journal of Applied Fluid Mechanics, Vol. 9, No. 6, pp. 2981-2992, 2016.
Available online at www.jafmonline.net, ISSN 1735-3572, EISSN 1735-3645.
DOI: 10.29252/jafm.09.06.26209

Numerical Simulation of Steady Supercavitating Flows

A. Jafarian and A. Pishevar†

Department of Mechanical Engineering, Isfahan University of Technology, Isfahan, 84156-83111, Iran

†*Corresponding Author Email: apishe@cc.iut.ac.ir*

(Received February 13, 2016; accepted May 11, 2016)

ABSTRACT

In this research, the Supercavitation phenomenon in compressible liquid flows is simulated. The one-fluid method based on a new exact two-phase Riemann solver is used for modeling. The cavitation is considered as an isothermal process and a consistent equation of state with the physical behavior of the water is used. High speed flow of water over a cylinder and a projectile are simulated and the results are compared with the previous numerical and experimental results. The cavitation bubble profile in both cases agrees well with the previous experimental results reported in the literature. As the result shows, coupling the two-phase Riemann solver with the considered EOS prepares a robust method for simulating the compressible fluid flow with cavitation which can undertake the whole physical behavior of water in a supercavitation process. Furthermore, the influence of the cavitator head and the flow speed on the supercavitation bubble is explored. The results show that cavitators with sharper head results in a smaller supercavitating bubble. Increasing the flow speed beyond a specific limit does not have any significant effect on the cavitation bubble and slightly increases the bubble size.

Keywords: Supercavitation; One-fluid method; Compressible flow; Multiphase flow; Equation of State.

1. INTRODUCTION

When a sudden pressure reduction occurs in liquid flow, the vapor cavities are generated. This is a usual phenomenon in compressible flows of liquids. Furthermore, many scientific and industrial processes deal with water as the main liquid medium. Water is a specific fluid with special thermodynamic properties for which the phase changes would be observed in many practical situations. Generally, water cavitation is an undesired situation and causes damages and malfunctions to a device. Pump propellers, hydrofoils of underwater vehicles, fuel injectors and etc. are some of these examples. On the other hand, the cavitation can have some important useful effects in some engineering cases in order to reduce the skin friction drag on an underwater body. When a solid body with sharp edges travels with a high speed in water, the cavitation vapor pocket envelopes the whole body and causes a considerable reduction in the skin friction drag. In this case, the great difference between the liquid and vapor viscosity is responsible for the drag reduction. Actually, the body is contact with the vapor instead of water and the physical behavior is called supercavitation (Zhang *et al*. 2010, Obikane *et al*. 2011, Shang 2013).

The intensity of a cavitation is determined by the cavitation number σ, defined as:

$$\sigma = \frac{P_\infty - P_{cav}}{\frac{1}{2}\rho U_\infty{}^2} \tag{1}$$

where P_∞ is the ambient pressure, P_{cav} is the constant cavitation pressure and U_∞ is the free stream velocity and ρ is the liquid density. When the cavitation number becomes very low ($\sigma << 0.1$) the flow enters the supercavitation regime (Savchenko 2001, Stinebring *et al*. 2001, Wu and Chahine 2007). As the definition implies, the stable supercavitation is achieved via a higher velocity or a smaller pressure difference. The smaller pressure difference is obtained by decreasing the ambient pressure or increasing the cavitation pressure through ventilating the cavity. Generally, the supercavitation divided into two main categories: The natural and artificial supercavitation. In the artificial supercavitation, the creation of the cavity bubble is assisted using the air ventilation.

In recent years, several investigations have been conducted toward the understanding of the physical behavior of the supercavitation phenomenon. Early studies in 80s, used the slender body theory to model the movement of the supercavitating projectiles (Wu and Chahine 2007, Tetsuo and

Khan 1981). In the 90 decade the investigations grown faster and more experimental and numerical methods used in supercavitation studies. In 1996 Savchenko experimentally investigated the motion of projectiles in a water tank. He explored the formation of supercavitation bubble behind a projectile in a velocity of 1360 m/s (Savchenko 1996). In 2001 Savchenko (Savchenko 2001) and Semonenko (Semenenko 2001) studied the natural and artificial supercavitation in horizontal, vertical and oriented motion while the projectile enters the water from the free surface. Serebryakov (Serebryakov and Schnerr 2003) used the asymptotic method and slender body theory in order to study the supercavitation around an axisymmetric body and modeled the hydrodynamic behavior of the flow in subsonic and supersonic regimes. In 2009 Zhang *et al*. explored the effect of the projectile geometry on the shape of the cavitation region. They used three different profiles for the head and different slope of the projectile body shape. Their experiments showed that the size of the supercavitation depends on the head profile and the body shape of the projectile (Zhang *et al*. 2009). Wu and Chahine (Wu and Chahine 2007) explored the shape of the supercavitation behind a body with different heads. They also tested the influence of air ventilation on the supercavitation size and found that the interface between the water and bubble is a great function of cavitator and ventilated air. Li *et al*. (Li *et al*. 2008) used the PIV technology to investigate the supercavitation bubble behind a hydrofoil in different cavitation number. In 2010 Lecysyn *et al*. (Lecysyn *et al*. 2010) studied the impact of a projectile to the high pressure tank and they investigated the influence of the supercavitation projectile movement on the tank pressure.

Recently, several numerical methods have been developed to simulate the occurrence of phase transition in the cavitating problems. There are two general approaches for modeling cavitating flow: the interface fitting method and the continuum modeling method. The first method assumes that there is a distinct interface between two phases which can be determined by an iterative method. This method is more useful for the problems in which the cavity is a closed volume or a pure gas. On the other hand, the continuum method treats the flow as a two phases with an average mixture density (Goncalves and Patella 2009). Furthermore, the continuum method is divided into two main categories: the one-fluid method and two-fluid method. Two-fluid method assumes that two phases exist in a computational cell simultaneously. Hence, the fluid flow is described using two sets of differential equations and exchanges between two phases are considered through source terms in the equations. On the contrary, one-fluid method uses one set of differential for the mixture and assume the two phases as a one fluid.This method is a powerful method for modeling the cavitation in compressible flows and simply simulates the creation, development and collapse of the cavitating bubble. The main challenge on this method is to find an appropriate equation of state which properly simulate all phase changes (Xie *et al*. 2006).

Different numerical methods have been used in the literature to simulate the supercavitating flows. Hu *et al*. (Hu *et al*. 2011) used the DCD method in order to simulate the supercavitating flow around a cylinder. They studied the effect of different equation of states in 2D and axisymmetric supercavitation. Zhu *et al*. (Zhu *et al*. 2012) used RKDG and WENO scheme to simulate the supercavitation around the cylinder. The one-fluid method with isentropic cavitation model was used and the velocity of the cylinder was set to 100 m/s. Hu *et al*. (Hu *et al*. 2013) simulated the supercavitation flow around the cylinder with different head cavitator. They investigated the effect of the velocity perturbation on the cavitation bubble. Zhang *et al*. (Zheng *et al*. 2013) used one-fluid method to explore the supercavitation phenomenon around a cylinder. They studied the interaction between the cavitation bubble and the shock wave.

This study aims to use a one-fluid method based on an exact two-phase Riemann solver to simulate the supercavitating flow around a moving body in water. This method uses an EOS which is consistent with the physical behavior of water in compressible cavitating flows. Here, in order to investigate the physical behavior of supercavitation and the design parameters in compressible cavitation, the unsteady supercavitating flow around a cylinder and a projectile are simulated and the effect of the cavitator head and the flow velocity on the supercavitation bubble is investigated.

The structure of this paper is as follows: the governing equations and the equation of state are presented in section 2, 3 and then the flow model used in this research is presented in section 4. The result for supercavitation modeling is presented in section 5 and the conclusion is presented in section 6.

2. GOVERNING EQUATIONS

Due to the dominance of convective terms over diffusion terms in high-velocity flows and because the time scale of viscosity is very larger than the wave propagation time scale, the diffusion terms in the Navier-Stokes equations are neglected and fluid flow is described using the Euler set of equations. The equations in conservation form are:

$$\frac{\partial U}{\partial t}+\frac{\partial F(U)}{\partial x}+\frac{\partial G(U)}{\partial y}=-\frac{n}{r}S(U) \tag{2}$$

$$U=\begin{bmatrix}\rho\\ \rho u\\ \rho v\end{bmatrix},\ F(U)=\begin{bmatrix}\rho u\\ \rho u^2+P\\ \rho uv\end{bmatrix},\quad G(U)=\begin{bmatrix}\rho v\\ \rho uv\\ \rho v^2+P\end{bmatrix},\ S(U)=\begin{bmatrix}\rho v\\ \rho uv\\ \rho v^2\end{bmatrix} \tag{3}$$

Which n for 2D and axisymmetric problems are 0 and 1, respectively. A suitable equation of state is needed to close the system of governing equations

which is discussed in the next section.

3. EQUATION OF STATE

As aforementioned in the previous section, the main challenge in one-fluid method for modeling cavitating flow is to implement an appropriate equation of state that could explain the phase transition in this phenomenon. Until now, many EOSs are presented for water in compressible flow in the context of one-fluid models.

The *cut off* model is one of the prominent models which is almost exclusively used for the simulation of the underwater explosions. No phase changes occurs in this model and it is a pure one-fluid model (Van Aanhold *et al*. 1998). When the pressure falls below the special value the pressure set to a known value – usually saturation vapor pressure. Despite its convenience for simulating, the *cut off* model suffers from many drawbacks. The conservation law may be violated, and the nature of hyperbolic systems of equations may change non-physically due to corresponding pressure and density cut-off or zero sound velocity in a cavitation zone (Liu *et al*. 2004). Schmidt *et al*. in 1990 used the assumption of homogenous and barotropic water mixture to present an equation of state base on integrating the predefined mixture sound speed equation. Schmidt model was first used for high-pressure and high-velocity cavitating flow in small nozzles (Schmidt *et al*. 1999). In fact, the Schmidt model can be employed for cases with small density ratio or cases in which the pressure jump across cavitation boundaries do not exceed a certain limit. This model is appropriate for the cases in which the medium pressure is high and the ratio $\rho_l / \rho_g < 10^{-5}$ is satisfied. Otherwise, this model results in a non-physically negative value. Thus, this method cannot cover the wide range of the compressible cavitating flow in which the ambient pressure is not very high. Another model which is presented by Liu *et al.* in 2004 is the *isentropic model* (Liu *et al*. 2004). This model is suitable for simulating the cavitating problems in compressible water flow and the proposed equation of state is based on an iterative method. The *isentropic model* is able to properly predict the size of the pressure peak and the wave propagation velocity. Hence, this model has been used in many cavitating simulations (Hu *et al*. 2011, Hu *et al*. 2013, Zheng *et al*. 2013, Zhu *et al*. 2012).

In order to compensate the weaknesses of the Schmidt equation of state, Xie *et al.* implement some modification on this model and presented a new model called *modified-Schmidt model.* In this model, the Schmidt equation of state is confined to a very short range of vapor fraction ($0<\alpha<0.02$) and the non-physical Schmidt's saturation pressure, P'_{sat}, is substituted with the physical P_{sat}. Furthermore, in order to avoid the negative pressure in cavitation zone, the negative pressure is substituted with $P_\varepsilon \approx 10^{-9}$. Using these modifications, the *modified-Schmidt* model can be used in wider range of the problems. This model was also coupled with the Euler equations to simulate the one- and two-dimensional cavitating flow in an underwater explosion. It should be mentioned that these modifications, exert some inconsistency in the numerical simulation and makes this model behave similar to the cut-off model. In addition, Dumbster *et al.* (Dumbser *et al*. 2013) used an interpolating scheme to obtain an equation of state for n-heptane and water from thermodynamics tables and simulated compressible mixtures of liquid and vapor, including the onset of cavitation.

In the present work, a new one-fluid model with a realistic equation of state for water is used for the cavitation problem in which the possibility of phase change is included in the solution of the Riemann problem. For this purpose, we assume that water is homogenous and barotropic and the phase change only takes place through an isothermal process, which is consistent with the physical conditions governing over cavitation in cold water and compressible flow.

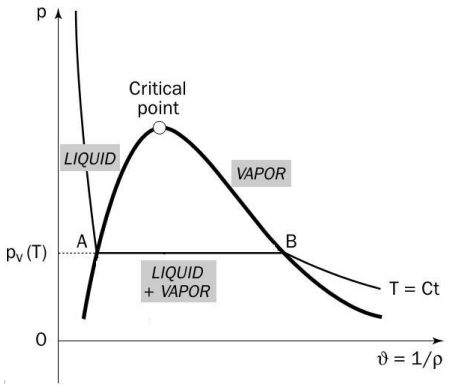

Fig. 1. Phase change in an isothermal process.

As Fig. 1 shows, when cavitation occurs, fluid can undergo a phase change from the subcooled liquid state to the vapor state on an isotherm line. For this reason, a barotropic equation of state is considered for water in this process as:

$$P = \begin{cases} (P_{sat} + B)\left(\dfrac{\rho}{\rho_l}\right)^{\alpha} - B & \rho > \rho_l \\ P_{sat} & \rho_g \le \rho \le \rho_l \\ {c_{vap}}^2 \rho & \rho < \rho_g \end{cases} \tag{4}$$

where the first relation in Eq. 4 is the Tait's equation of state for which $\alpha = 7.15, B = 3.309 \times 10^8$ and the temperature of water is set to be T=25°C. For the other parameters we have $P_{sat} = 3169\,Pa$; $\rho_l = 1000\,kg/m^3$; $\rho_g = 0.01\,kg/m^3$ and $c_{vap} = 660\,m/s$.

4. CAVITATION MODEL

Most numerical methods encountered discontinuous

solution in compressible flow problems need to solve a Riemann problem across the cell boundaries (Pishevar 2006). In fact, the Riemann problem, examines the flow obtained from the Euler equation with a discontinuous initial condition as:

$$U_{t=0} = \begin{cases} H_l & x < 0 \\ H_r & x > 0 \end{cases} \quad (5)$$

where H_r and H_l are the constant states on the right and left of an interface. Unfortunately, there is no closed analytical solution even for the simplest case of an ideal gas for this problem. Therefore, the methods to solve a Riemann problem are categorized into Approximate Riemann Solvers and Iterative Riemann Solvers. Methods such as Roe, HLL, HLLC and others can be acknowledged as Approximate Riemann Solvers. Reference (Toro 2009) provides more accurate information concerning these methods. Iterative method is another method that can be applied for solving the Riemann problem more accurately; however, only a few solutions have been proposed for special cases so far.

In the one-fluid method used in this research for calculating the cavitation zones in water, a new wave pattern is assumed for the resolution of a Riemann problem which is consistent with the physical nature of the cavitation in compressible flow and the cavitation is considered as an equilibrium phenomenon in each time step. According to the isothermal barotropic EOS, the wave pattern should consist of the phase transition during the cavitation. Figure 2 depicts the general wave pattern while the initial left and right conditions leads to a cavitation zone.

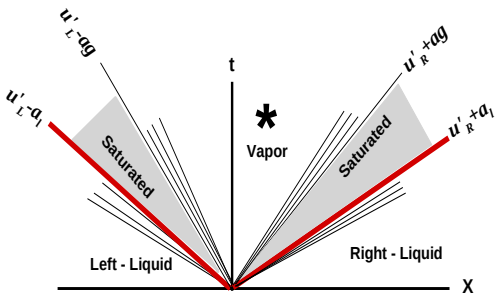

Fig. 2. Wave pattern in the Riemann problem.

In this figure two strong expansions are occurred and the cavitation is created in the middle states. According to Eq. 4, each rarefaction wave is divided into two parts. The first part of the rarefaction is assigned to the liquid phase and the other is in the vapor phase. As illustrated by Fig. 2 the phase transition is occurred through an evaporation wave (red line) and the liquid state changes into a two phase state. For cases that the intermediate pressure is reduced to a value less than the vapor pressure, a new rarefaction wave appears in the wave pattern through which the two phase state changes into the vapor state.

4.1 Strategy to Solve the Riemann Problem

In order to construct a multiphase wave pattern for the resolution of the Riemann problem when the left and the right initial conditions lead to a cavitation zone in water, we assume that the expansion waves in liquid and vapor phases are isothermal waves and the pressure remains constant in the saturation dome. When an expansion wave propagates in the liquid phase, the water pressure decreases below the saturation pressure P_{sat}. Then the liquid phase transforms to vapor phase in an isobaric process by an evaporation wave and cavitation occurs. As Fig. 2 depicts, the speed of the evaporation wave is considered to be equal to the speed of the last wave in the liquid expansion fan. Across the evaporation wave, density will jump from ρ_l to the ρ_g while the flow speed remains constant. It should also be noted that pressure wave is not allowed to propagate within a fluid in the saturated state. If the initial condition in a Riemann problem leads to a stronger expansion, we move to the vapor branch on the p-v diagram and the expansion continues with isothermal waves in the water vapor phase. In this paper the water vapor phase is assumed as an ideal gas, which is consistent with the physical properties of water in these criteria.

In our model three different phases can be considered for water in the Riemann problem. Based on the left, right and intermediate (*) initial states, the resolution to the Riemann problem for our model consists of 27 different wave patterns. Some of the essential patterns are presented in Fig. 3 which shows how left and right condition can be connected to the intermediate states.

In Fig. 3, *R* and *S* symbols on the wave patterns stand for the rarefaction and shock wave, respectively, and * symbol is related to the intermediate zone. In the following, a five step algorithm is proposed to determine the intermediate state of a multiphase Riemann problem. These steps are:

Step1: Using the Left and Right initial condition to categorize the general wave pattern.

Step2: Using the Shock/Rarefaction relations to define the criteria for saturation condition in the * region.

Step3: Define the algebraic relation $F(P^*, P_L, P_R, u_L, u_R) = 0$ for the P^*.

Step4: Define the derivation of function *F*.

Step5: Solving the algebraic equation for P^* using the Newton method.

Using this five step algorithm, one can obtain the pressure in the intermediate state and other quantities such as density and velocity will be defined consequently.

4.2. Numerical Method

In this paper, a cell centered finite volume method is used for discretizing the compressible flow equations for water. In order to easily deal with the

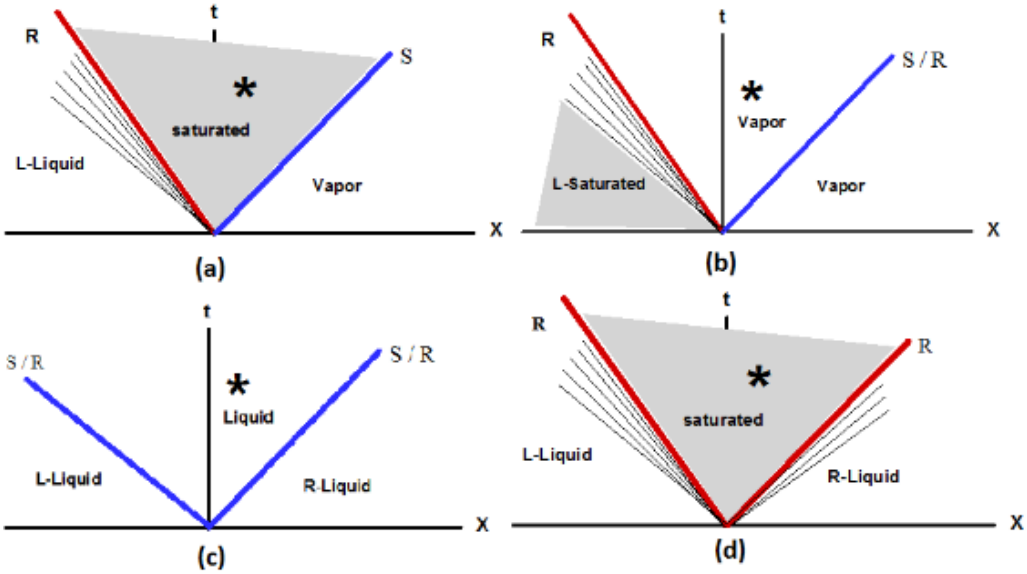

Fig. 3. Different wave patterns for the multiphase Riemann problem.

geometry, a triangular mesh is used. Furthermore, the second order Godunov method coupled with an exact Riemann solver is used for calculating the flux vector on each edge of a computational cell (Pishevar 2006). The time step is calculated according to the CFL condition and the characteristic length of the mesh size and the minimum allowable time evaluated for the whole domain is applied as the integration time step.

4.3. Boundary condition

In order to enforce the appropriate condition at each boundary a virtual cell is used. Then the numerical flux at a boundary edge is obtained in the same way as it is obtained for an internal edge. Fig. 4 depicts the virtual cell and the according velocity components.

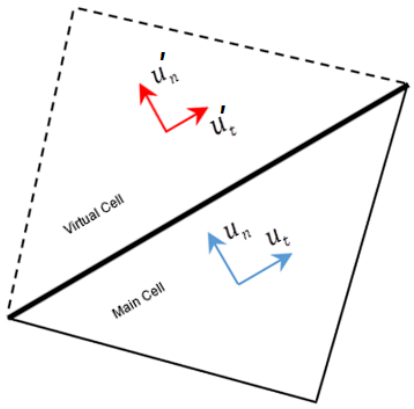

Fig. 4. Virtual cells on the boundaries.

In this research the characteristic method is used to set the flow states for virtual cells. At the inlet boundary, the free stream velocity is assigned to the inlet virtual cells and other quantities are extrapolated from inside of the domain. For the outlet boundary, the velocities are the same as the main cells and the density and pressure are assigned from the free stream condition. On the other hand, the state of the far-field virtual cells are set to the free stream conditions. Finally, the reflective boundary condition is implemented at the solid and symmetric boundaries.

5. RESULTS

In this section, in order to illustrate the capability of the presented model, the shock tube problem with an initial condition which resulted in strong cavitation is simulated and the results are compared with the modified Schmidt model. After that, a standard test case, the problem of supercavitating flow over a cylinder is simulated and the result is compared with the analytical and other numerical methods. Then, the supercavitating flow around a projectile is simulated and the cavitation bubble is compared with the experimental results. Finally, the effects of the cavitator head shape and the flow speed on the cavitation bubble are studied for several cases.

5.1. Shock Tube Problem with a Cavitating Zone

In order to verify the capability of the presented model, the one-dimensional shock tube problem with cavitation is simulated and the results are compared with modified-Schmidt model. Here, the shock tube is initially filled with subcooled water. The left and the right side of the domain have the initial condition as below:

$$U_L = \begin{bmatrix} 1010 \\ -200 \end{bmatrix}; U_R = \begin{bmatrix} 1010 \\ 200 \end{bmatrix}$$

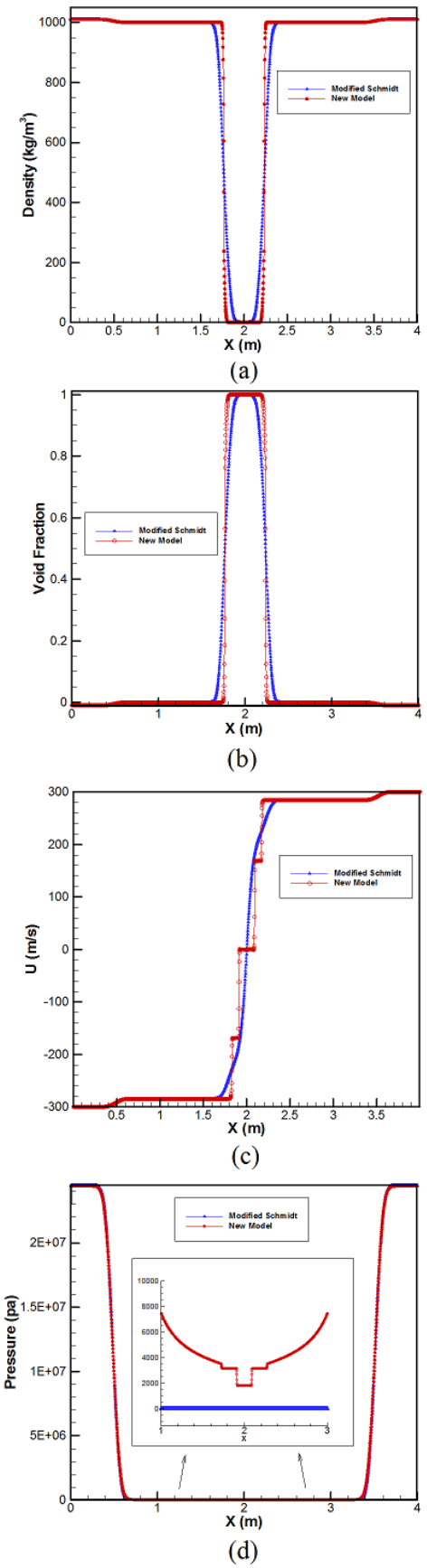

Fig. 5. Diagrams of density, volume fraction, velocity and pressure at t=0.8 *ms* for 1D shock tube problem.

This initial condition is resulted in a sudden expansion with onset of cavitation in the middle of the shock tube. The length of the domain is 4 *m*, and 2000 computational nodes are used in this simulation. Density, void fraction, velocity and pressure variation are shown in Fig. 5 at t=0.8 *ms*. The void fraction is calculated as: $Void\ fraction = \dfrac{\rho - \rho_g}{\rho_l - \rho_g}$.

The wave pattern presented in Fig. 2 completely illustrates the variation of vector quantities in this simulation. As this figure shows, two rarefactions emanate from the middle of the shock tube and move toward each side of the domain. The propagation of two waves, decreases the density and the pressure from the liquid phase to the vapor phase. The variation of the pressure and velocity clearly illustrates the phase transition across the rarefaction wave. As Fig. 5 shows, because the modified-Schmidt model consider the phase transition as a single liquid phase, this model is not able to distinguish each phase during the phase transition. Finally, the size of the cavitation region predicted by the present model is smaller than the modified-Schmidt model.

5.2. Supercavitation flow over a Blunt Cylinder

In the first problem the axisymmetric supercavitating flow over a blunt cylinder is simulated. The length and diameter of the cylinder are 200 *mm* and 10 *mm*, respectively.

Figure 6 depicts the computational domain covered with the triangular cells and the corresponding boundary conditions. The length and the width of the domain are 1.2 *m* and 0.8 *m*, respectively.

In this simulation a grid of 59471 computational nodes is used for the modeling. The value of time step is in the order of $O(10^{-8})$ and the computer simulation on an Intel 2.3 *GHz* CPU take about 43 hours. As Fig. 6 illustrates, very fine elements are used near the cylinder and the cell size is gradually increased by approaching to the far-field and inlet boundaries.

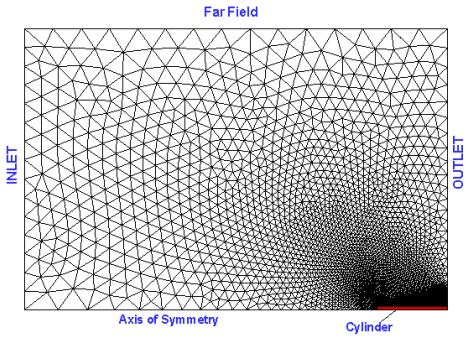

Fig. 6. Computational domain and boundary conditions.

The initial flow parameters are set as $U_\infty = 100\,m/s$, $P_\infty = 10^5$ Pa, $\rho_\infty = 1000.041$ kg/m^3 and the cavitation number is $\sigma = 0.02$. The

Mach number is calculated according to the sound velocity in the liquid medium and $M = U_\infty / a = 0.065$. The formation of cavitation bubble is shown in Fig. 7 by the density contours. As Fig. 7 depicts the cavitation bubble forms from the sharp tip of the cylinder and develops during the time to finally envelope the total geometry of the cylinder.

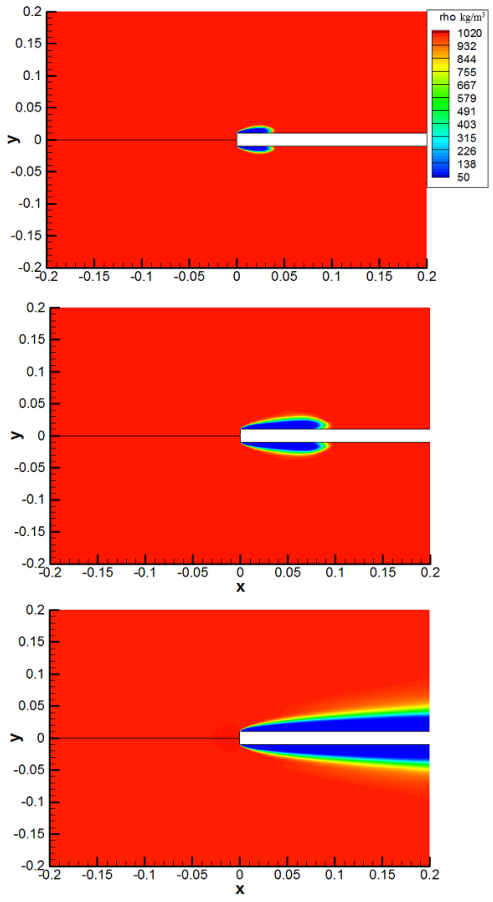

Fig. 7. Formation and development of supercavitation bubble over the cylinder.

There are some analytical and numerical solutions for this problem. Fig. 8 shows the comparison between the cavitation bubble profiles. As this figure depicts, the cavitation profile simulated in the present method agrees well with the Hu *et al*. (Hu *et al*. 2013) results and Munzer-Richardt theory (Grady 1979). Here, Hu *et al*. used the compressible one-fluid method and the isentropic equation of state for simulating the supercavitation flow and the Munzer-Richardt theory used the analytic potential flow to estimate the cavitation region in supercavitating bubble profile. In this theory, the radius of the cavitation bubble in an axisymmetric flow will be obtained by

$$R_c(x) = R_{\max}\left[\frac{4x}{L_{\max}(1-\frac{4x}{L_{\max}})}\right]^{1/2.4} \quad (6)$$

where R_c is the cavitation radius at the location of x from the tip of the body and the cavitation is generated from the nose of the body. The maximum length and radius are respectively given by:

$$L_{\max} = 2r\sqrt{C_d(\sigma)/\sigma^2 \ln(1/\sigma)}$$
$$R_{\max} = r\sqrt{C_d(\sigma)/\sigma}$$

where r, σ and C_d are the cavitator radius, cavitation number and cavitator drag coefficient respectively and the cavitator drag coefficient is obtained by $C_d(\sigma) = C_{d0}(1+\sigma)$ and C_{d0}=0.815.

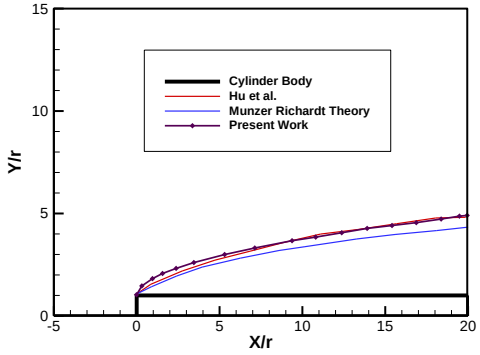

Fig. 8. Comparison between the numerical and analytical supercavitation profile.

5.3. Supercavitation flow Over an Underwater Projectile

As the second validating test case, supercavitating flow over an underwater projectile is simulated. The projectile is a cone with a blunt disc head shape. The schematic geometry of the projectile is shown in Fig. 9. The radius of the cavitator head is 0.71*mm*, the length of the projectile is 157.4 *mm* and the radius of the end part is 6.6 *mm* and the apex angle of the body is 2.1º. Some experimental data was presented by Hrubes (Hrubes 2001) for this geometry. The experimental information are prepared using the high speed imaging for exploring the supercavitating flow. Since the depth of water in the experiment was 4 *m*, the ambient pressure is considered to be $P_\infty = 1.4\times10^5 Pa$ in this study. Moreover, the initial velocity is set to $U_\infty = 970 m/s$ and the Mach number is M=0.64 and the density and cavitation number are $\rho_\infty = 1000.06\ kg/m^3$ and $\sigma = 2.9\times10^{-4}$. The length and the width of the computational domain is 2.2 *m* and 0.8 *m*, respectively and the projectile is placed at x=0 *m* (Fig. 10). The boundary conditions are exactly similar to the previous problem and the computational grid consists of 119289 triangular cells. The average time step size for this simulation is in the order of $O(10^{-9})$ and the total CPU time is about 68 hours.

Figure 11 shows the density contours for this problem. As this figure shows, a conical ring of vapor envelopes the whole projectile body. Furthermore, Fig. 12 shows experimental shadowgraph of the projectile and the cavitation

bubble around the body. The simulated bubble profile agrees well with the experimental data.

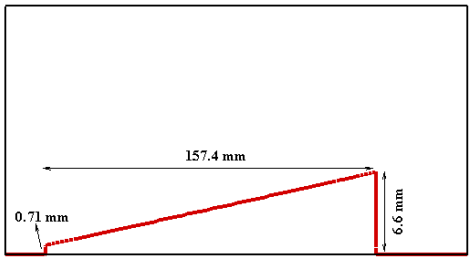

Fig. 9. Schematic shape of the projectile with the apex angle of 2.1º.

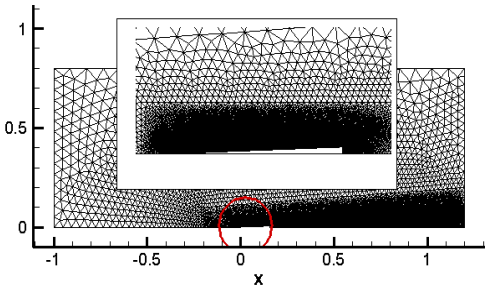

Fig. 10. Schematic geometry and the triangular mesh of the computational domain.

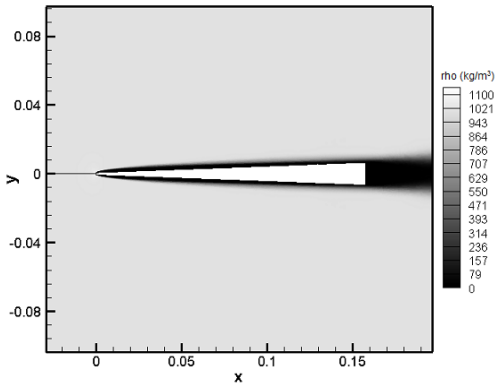

Fig. 11. Density contour for supercavitating flow over the projectile.

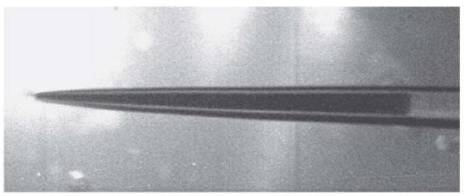

Fig. 12. Shadowgraph of the supercavitating projectile.

The creation of the supercavitation bubble behind the projectile is presented in Fig. 13. As Fig. 13-a shows, the simulated cavitation bubble is stretched behind the projectile and the radius of the supercavitating bubble grows slightly to the end of the computational domain. This phenomenon also can be seen in the experimental result presented in Fig. 13-b.

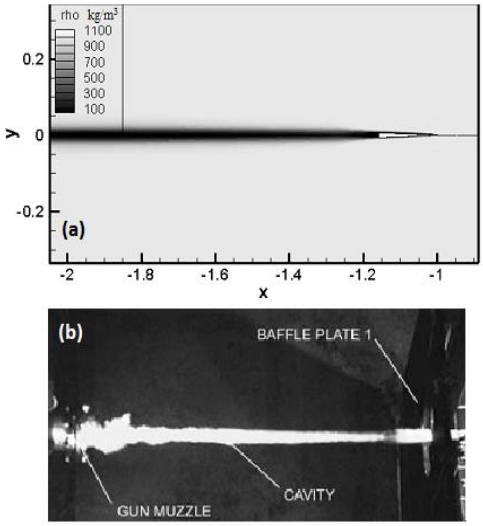

Fig. 13. (a) Simulated supercavitation profile behind the projectile (b) The experimental shape of supercavitation profile behind the projectile.

The comparison between the present work and the analytical and experimental data is presented in Fig. 14. As shown by this figure, the simulated cavitation profile agrees well with the experimental data and the Munzer-Richardt theory predicts a larger bubble profile.

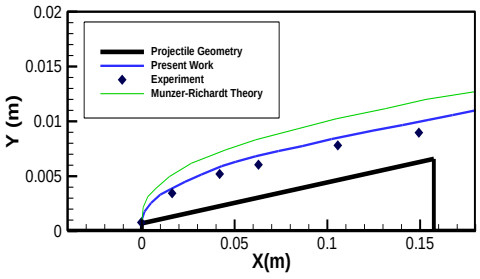

Fig. 14. Comparison between the present work bubble profile and the analytical and experimental results for supercavitation bubble over the projectile.

In this study the flow is assumed to be inviscid and the Euler equations are used for the simulation. Hence, the viscous forces cannot be computed directly. However, to quantitatively show the overall effects of supercavitation on the drag force, we use an approximate integral method –Thwaites method - to evaluate the viscous drag force. For this purpose, the velocity at the boundary layer edge U is obtained from the numerical simulation at each station and the other Thwaites parameters are determined using this velocity.

In order to investigate the effect of supercavitation, both sharp and blunt projectiles are simulated and the viscous and pressure drag forces are computed separately. Because there is a significant difference

between the vapor and liquid viscosity the viscous forces are different for several order of magnitude. The Table 1 illustrates the effect of the supercavitation design on the pressure, viscous and total drag forces.

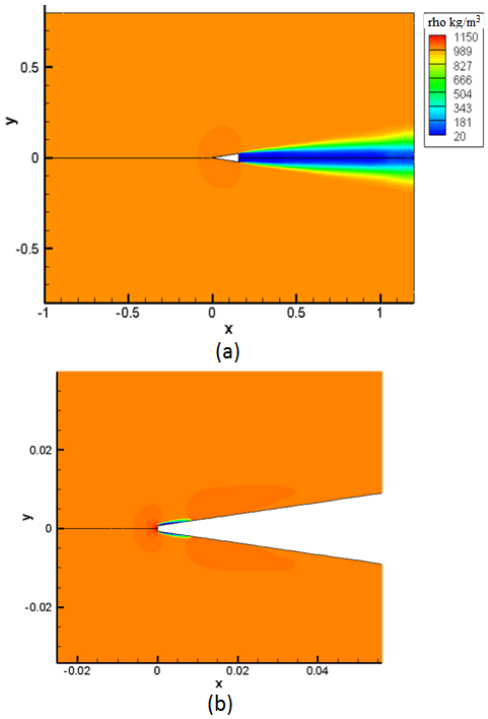

Fig. 15. Flow density contours around the projectile with an apex angle of 8.4º (a) the cavitation behind the projectile (b) the cavitation near the tip of the projectile.

The total drag force in Table 1 shows the effect of the supercavitation and the extra pressure drag force generated in the blunt design is compensated by the effect of the vapor viscosity and the viscous drag force.

Table 1 Comparison between the viscous and pressure drag force for sharp and blunt projectiles

Projectile head	Pressure Drag (N)	Viscous Drag (N)	Total Drag (N)
Sharp	367.3	462.5	829.8
Blunt	650	2.3	652.3

In order to explore the influence of the projectile body profile, the simulation is conducted with the same flow condition, but with a different shape for the projectile. Here, the size of the cavitator head and the length of the body are similar to the previous shape, but the radius of the end part is increased to 24 *mm*. In other words, the projectile apex angle is increased to 8.4º. Fig. 15 shows the cavitation regions created in the supercavitating flow around this projectile. In this case, the cavitation bubble does not envelope the whole body and only a cavitation pocket is formed near the tip of the cavitator (Fig. 15-b). Here, the slope of the projectile body causes a considerable increase in the pressure field near the projectile and the cavitation region fades quickly after the tip of the cavitator. Actually the radius of cavitator head and the slope of the body have an opposite influence on the cavitating bubble. The larger radius of the cavitator head causes the larger supercavitating bubble, while the larger apex angle of the body increases the pressure field near the body. An enveloping supercavitating bubble is possible if the cavitator radius is increased, but the larger cavitator head causes a drastic increase in the pressure drag coefficient which is not suitable in the design of a projectile. This phenomenon demonstrates that the body profile plays an important role in the design of the supercavitating projectiles and all these parameters should be considered.

In order to compare the influence of the apex angle of the body on the pressure field, the pressure filed in both 2.1º and 8.4º are presented in Fig. 16. The upper half of this figure shows the pressure field resulted from the projectile with apex angle of 8.4º. This figure clearly reflects the effect of body slope on the pressure field. In the upper case, the pressure field is completely affected by the body and a high pressure zone is generated around the projectile. In this case, the radial velocity near the tip of the projectile and the separation of the flow cause a little decrease in the pressure around the tip of the projectile head. On the other hand, the expansion of the flow in the projectile with the apex angle of 2.1º cause the reduction of the pressure along the whole body and this pressure reduction is dominant in this case and the supercavitating bubble envelope the total length of the projectile. In addition, in order to seek a deeper insight about the effect of the body design, the pressure drag force and pressure drag coefficient are presented in Table 2. The pressure drag force is increased drastically as a result of increasing the slope of the projectile body.

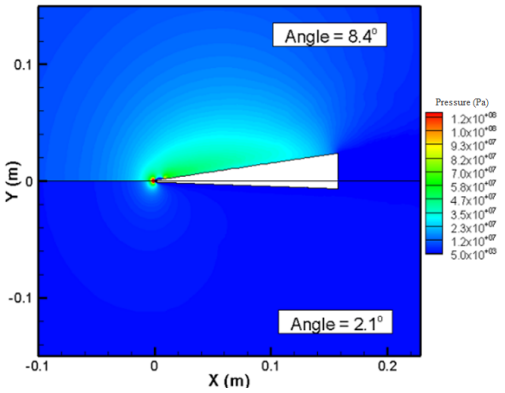

Fig. 16. Comparison between the pressure field in supercavitating flow (up) apex angle = 4.8º (down) apex angle = 2.1º.

5.4. Effect of Cavitator Shapes

In this section the influence of the cavitator head on the supercavitation profile is explored. Here, a cylinder with four different cavitator heads are simulated. In all cases the velocity is 100 *m/s* and

$P_\infty = 10^5 Pa$. Three sharp conic head with different aspect ratios and a round head are modeled. Fig. 17 depicts the schematic shape of the conic cavitator head. The simulations are conducted for $L_{tip}/r = 1, L_{tip}/r = 2.5, L_{tip}/r = 5$.

Table 2 Pressure drag force and pressure drag coefficient for the projectile with different apex angles

C_D	F_D (N)	Projectile geometry
0.010	650	angle = 2.1°
0.057	50450	angle = 8.4°

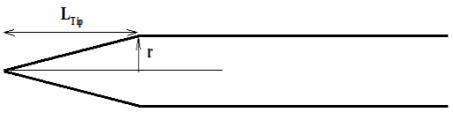

Fig. 17. A schematic of cylinder with sharp cavitator.

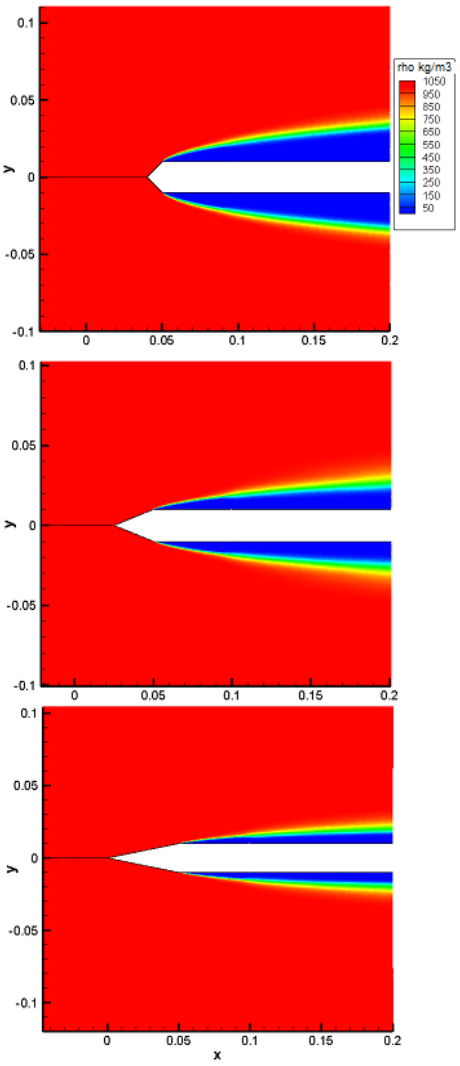

Fig. 18. Density contours for supercavitation flow around the cylinder with a conical head (a) $L_{tip}/r = 1$ (b) $L_{tip}/r = 2.5$ (c) $L_{tip}/r = 5$.

Figure 18 and 19 show the cavitation bubble for the different cavitator heads. As the density fields illustrate, in all cases the supercavitation bubble envelope the whole cylinder body and for all aspect ratios the cavitation is created from the sharp edge connecting the head and the main horizontal body (Fig. 18). Fig. 19 illustrates the comparison between the supercavitation profiles in different conical angles. This figure shows that, the larger is the aspect ratio (L_{tip}/r), the thinner is the cavitation bubble profile. The radial component of the velocity is decreased in larger aspect ratios, hence the cavitated zone around the cylinder is shrunk.

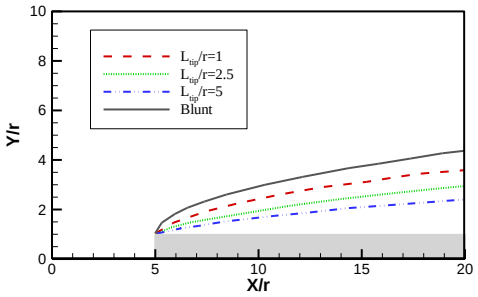

Fig. 19. Cavitation bubble profiles for a cylinder with different conical head.

In another case, the simulation is conducted for the cylinder with a round cavitator head. Fig. 20 shows the density contour for this case. Contrary to the conical head, the location of the cavitation bubble does not start from the main body and the size of the cavitation bubble is smaller than the blunt cylinder. Figure 21 compares the bubble start point and the size of the cavitation bubble for the round and blunt cylinders.

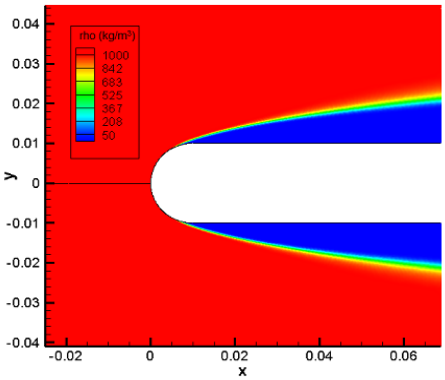

Fig. 20. Density contour in supercavitation flow around a cylinder with a round head.

Similar to the projectile, the pressure drag coefficient are calculated for the cylinder with different cavitator heads. As Table 3 illustrates, the blunt cavitator and the conical head with $r_{Cylinder}/L_{Tip} = 1/5$ has the maximum and minimum drag coefficients respectively. Furthermore, the drag coefficient of the round cavitator is less than the conical head with $r_{Cylinder}/L_{Tip} = 1$.

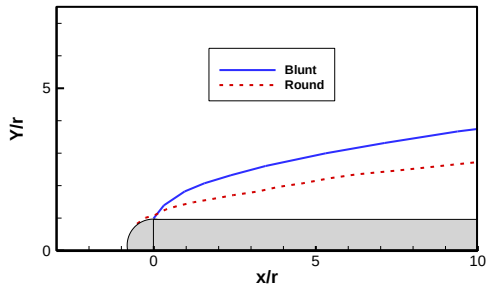

Fig. 21. Cavitation profile around the cylinder with blunt and round head.

Table 3 Pressure drag coefficient for cylinder with different cavitator head

C_D	Cavitator head profile
0.783	Blunt
0.283	Round
0.014	Conic $r_{Cylinder} / L_{Tip} = 1/5$
0.071	Conic $r_{Cylinder} / L_{Tip} = 1/2.5$
0.325	Conic $r_{Cylinder} / L_{Tip} = 1$

5.5. Effect of Flow Speed

In this section the effect of the flow speed on the supercavitation flow around the cylinder is explored. All parameters of the flow are kept constant and the inlet density and pressure are $\rho_\infty = 1000.041 kg/m^3$ and $P_\infty = 10^5 Pa$ respectively. The simulations are conducted for the cylinder with blunt and round head.

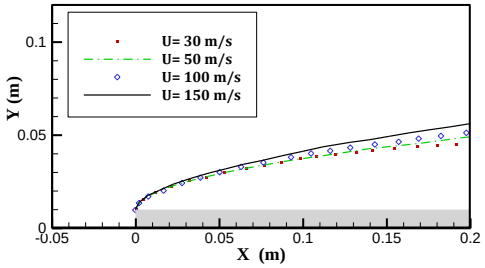

Fig. 22. Comparison between the supercavitating profiles around the blunt cylinder in different velocities.

The supercavitating flow around the blunt cylinder is simulated in four different velocities U_∞ =30,50,100,150 *m/s*. Fig. 22 shows the comparison between the supercavitation bubble profile created around the cylinder. As this figure shows by increasing the inlet velocity, the larger cavitating bubble will be achieved. Furthermore, we repeated these simulations for the cylinder with the round head in three velocities u=50,100,150 *m/s*. As Fig. 23 depicts, the similar results are obtained for the round cavitator head. It should be noted that, although by increasing the inlet velocity a larger supercavitation bubble profile is resulted, the difference between the profiles are not significant. As the results shows, the velocity of blunt cylinder is increased up to five times of the initial velocity, but the cavitation profile grows slightly in compare to the initial profile. Hence, the influence of the inlet velocity on the supercavitation bubble profile is not significant and its effect on the separation point is almost negligible.

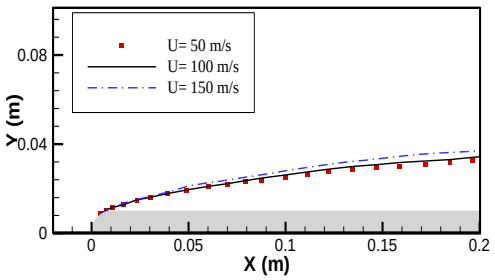

Fig. 23. Comparison between the supercavitating profiles around the cylinder with round head in different velocities.

6. CONCLUTION

In this research, supercavitation in compressible water flow is explored. The one-fluid method is coupled with the two-phase Riemann solver and a new wave pattern is proposed for the flow simulation. Because of high velocity the effect of viscous terms is neglected. First, the supercavitation phenomenon around a blunt cylinder traveling with 100 *m/s* in water was simulated and the obtained cavitation bubble profile had a good agreement with the other analytical and numerical results. In another case the supercavitating flow over the projectile in 970 *m/s* was modeled and the predicted bubble profile around and behind the projectile agreed well with experimental results. Finally, the effect of the cavitator head and inflow velocity on the supercavitation profile was investigated. A cylinder with three conic head and a round head were simulated. The results showed that the sharper conic head results in a smaller supercavitation bubble. In addition, increasing the inlet velocity resulted in a larger supercavitation bubble but the influence of the inlet velocity was not significant.

REFERENCES

Dumbser, M., U. Iben and C. D. Munz (2013). Efficient implementation of high order unstructured WENO schemes for cavitating flows. *Computers and Fluids* 86, 141-168.

Goncalves, E. and R. F. Patella (2009). Numerical simulation of cavitating flows with homogeneous models. *Computers and Fluids* 38(9), 1682-1696.

Grady, R. J. (1979). Hydroballistics Design Handbook, Vol I, Naval Sea Systems Command 38-45. Technical Report No. SEAHAC/79-1.

Hrubes, J. D. (2001). High-speed imaging of supercavitating underwater projectiles. *Experiments in Fluids* 30(1), 57-64.

Hu, Z., H. Dou and B. Khoo (2011). On the modified dispersion-controlled dissipative (DCD) scheme for computation of flow supercavitation. *Computers and Fluids* 40(1), 315-323.

Hu, Z., B. Khoo and J. Zheng (2013). The simulation of unsteady cavitating flows with external perturbations. *Computers and Fluids* 77, 112-124.

Lecysyn, N., A. Bony-Dandrieux, L. Aprin, F. Heymes, P. Slangen, G. Dusserre, L. Munier and C. Le Gallic (2010). Experimental study of hydraulic ram effects on a liquid storage tank: Analysis of overpressure and cavitation induced by a high-speed projectile. *Journal of Hazardous Materials* 178(1), 635-643.

Li, X., G. Wang, M. Zhang and W. Shyy (2008). Structures of supercavitating multiphase flows. *International Journal of Thermal Sciences* 47(10), 1263-1275.

Liu, T., B. Khoo and W. Xie (2004). Isentropic one-fluid modelling of unsteady cavitating flow. *Journal of Computational Physics* 201(1), 80-108.

Obikane, Y., M. Kaneko, K. Kakioka and K. Ogura (2011, June). Image analysis of fine structures of supercavitation in the symmetric wake of a cylinder. *WASET, proceedings*, Paris.

Pishevar, A. (2006, September). An ALE scheme for numerical simulation of 2D underwater explosion. In ECCOMAS CFD 2006: Proceedings of the European Conference on Computational Fluid Dynamics, Egmond aan Zee, The Netherlands, Delft University of Technology.

Savchenko, Y. N. (1996). Motion in water at supercavitation speeds. *International Journal of Fluid Mechanics Research* 23(1-2).

Savchenko, Y. N. (2001). Experimental Investigation of Supercavitating Motion of Bodies, Ukrainian Academy of Sciences Kiev Inst of Hydromechanics.

Savchenko, Y. N. (2001). Supercavitation Problems and Perspectives. *4th International Symposium on Cavitation*, California Institute of Technology Pasadena, California.

Schmidt, D. P., C. J. Rutland and M. L. Corradini, (1999). A fully compressible, two-dimensional model of small, high-speed, cavitating nozzles. *Atomization and sprays* 9(3), 255-276.

Semenenko, V. N. (2001) Artificial Supercavitation. Physics and Calculation. RTO AVT Lecture Series on "Supercavitating Flows," Brussels, Belgium.

Serebryakov, V. and G. Schnerr (2003, November). Some Problems of hydrodynamics for sub-and supersonic motion in water with supercavitation. In *Fifth international symposium on cavitation*, CAV2003, Osaka, Japan, 1-19.

Shang, Z. (2013). Numerical investigations of supercavitation around blunt bodies of submarine shape. *Applied Mathematical Modelling* 37(20), 8836-8845.

Stinebring, D. R., M. L. Billet, J. W. Lindau and R. F. Kunz (2001). *Developed Cavitation-cavity Dynamics*. Pennsylvania State University Park Applied Research Lab.

Tetsuo, N. and O. F. Khan (1981). Compressibility effects on cavitation in high speed liquid flow: second report-transonic and supersonic liquid flows. *Bulletin of JSME* 24(190), 655-661.

Toro, E. F. (2009) Riemann solvers and numerical methods for fluid dynamics: a practical introduction. *Springer Science and Business Media*. 293-306

Van Aanhold, J., G. Meijer and P. Lemmen (1998). Underwater shock response analysis of a floating vessel. *Shock and Vibration* 5(1), 53-59.

Wu, X. and G. L. Chahine (2007). Characterization of the content of the cavity behind a high-speed supercavitating body. *Journal of Fluids Engineering* 129(2), 136-145.

Xie, W., T. Liu and B. Khoo (2006). Application of a one-fluid model for large scale homogeneous unsteady cavitation: The modified Schmidt model. *Computers and Fluids* 35(10), 1177-1192.

Zhang, B., Y. W. Zhang and X. L. Yuan (2009). Effects of the profile of a supercavitating vehicle's front-end on supercavity generation. *Journal of Marine Science and Application* 8(4), 323-327.

Zhang, J. Z., Zhang, J. S., & Wei, Y. J. (2010, June). Simulation of tail-slap loads of supercavitating projectiles. In 2010 Third International Conference on Information and Computing, Vol. 2, 163-166.

Zheng, J., B. Khoo and Z. Hu. (2013). Simulation of wave-flow-cavitation interaction using a compressible homogenous flow method. *Commun. Comput. Phys.* 14(2), 328-354.

Zhu, J., T. Liu, J. Qiu and B. C. Khoo (2012). RKDG methods with WENO limiters for unsteady cavitating flow. *Computers and Fluids* 57, 52-65.